Engineering Applications of Artificial Intelligence 122 (2023) 106007

Contents lists available at ScienceDirect

Engineering Applications of Artificial Intelligence

journal homepage: www.elsevier.com/locate/engappai

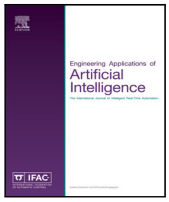

International Roughness Index prediction for flexible pavements using novel machine learning techniques

Mosbeh R. Kaloop [a,b,c], Sherif M. El-Badawy [c], Jong Wan Hu [a,b,*], Ragaa T. Abd El-Hakim [d]

[a] Department of Civil and Environmental Engineering, Incheon National University, South Korea
[b] Incheon Disaster Prevention Research Center, Incheon National University, South Korea
[c] Public Works Engineering Department, Faculty of Engineering, Mansoura University, Egypt
[d] Public Works Engineering Department, Faculty of Engineering, Tanta University, Egypt

ARTICLE INFO

Keywords:
IRI
Flexible pavement
LTPP
MLR
GPR
ANN
PSO
ANFIS
LWP

ABSTRACT

International Roughness Index (IRI) is an important pavement performance indicator that is widely used to reflect existing pavement condition and ride quality. Due to the importance of this significant index, the current research aims to develop a precise IRI prediction model using the Gaussian Process Regression (GPR) and Locally Weighted Polynomials (LWP). The long-term pavement performance (LTPP) datasets of pavement age, initial IRI, alligator, longitudinal and transverse cracks, standard deviation of rutting, and subgrade plasticity index variables are employed in predicting IRI. These datasets are collected from 126 different flexible pavement sections of the LTPP specific pavement studies (SPS-1) located in different climatic zones in the US. The total number of IRI measurements in the collected database is 925 which covers a wide range of IRI values. Multiple linear regression (MLR) is firstly applied to classify the input variables. Then the MLR model is compared with four machine learning techniques which are GPR, LWP, Particle Swarm Optimization-Adaptive Network based Fuzzy Inference System (PSO-ANFIS) and PSO-Artificial Neural Networks (PSO-ANN). The developed models' performance is validated using different statistical indices, including the coefficient of determination (R^2). The results demonstrate that the GPR ($R^2 = 0.93$) and LWP ($R^2 = 0.90$) outperformed the PSO-ANFIS ($R^2 = 0.65$) and PSO-ANN ($R^2 = 0.52$) in predicting IRI. Thus, the GPR model is found to be more accurate for IRI modeling compared to the hybrid investigated models.

1. Introduction

As the pavement structure ages, it suffers from different distresses, some of which are load induced distresses, while other are climate related distresses. Longitudinal and alligator fatigue cracking in flexible pavements are load-associated distresses which occur due to repeated traffic loads. On the other hand, the main reasons for potholes and transverse cracks are non-load sources such as the moisture and low temperature impacts, respectively (Hossain et al., 2019). Other types of distresses are rutting, raveling, bleeding, ... etc. Due to the distortion of the pavement surface combined with cracks, the pavement surface may become rougher which affects the ride comfort of road users. Thus, Departments of Transportation (DOTs) in most developed countries frequently monitor and evaluate the condition of the existing road network to define any functional and/or structural defects as the network ages (Hossain et al., 2019; Abdelaziz et al., 2020). International Roughness Index (IRI) which is reported to be a function of different pavement distresses is commonly used to exhibit the pavement functional condition and ride quality (Elhadidy et al., 2021; Hossain et al., 2019; OBrien et al., 2018). Thus, accurate measurement or prediction of IRI is essential for an effective pavement management system.

Many research efforts were devoted towards predicting IRI through traditional techniques such as regression, and/or machine learning techniques such as Artificial Neural Networks or other machine or deep learning techniques. However, some of these models lack robust measured comprehensive database, or suffer from modeling accuracy issues. Therefore, the current research paper aims to use a comprehensive measured reliable database to accurately predict IRI using innovative machine learning techniques.

2. Literature related research

Traditionally, many researchers have tried to model IRI as a function of the pavement distresses using the classical regression modeling techniques (Abdelaziz et al., 2020; ARA, 2008; National Cooperative Highway Research Program (NCHRP 1-37A), 2004; Pérez-Acebo et al., 2021). Multiple Linear Regression (MLR) was used to predict flexible and rigid pavements IRI based on Laos Road Management System

* Corresponding author at: Department of Civil and Environmental Engineering, Incheon National University, South Korea.
E-mail address: jongp24@inu.ac.kr (J.W. Hu).

https://doi.org/10.1016/j.engappai.2023.106007
Received 28 August 2022; Received in revised form 24 November 2022; Accepted 14 February 2023
Available online 13 March 2023
0952-1976/

(RMS) database and its performance was found acceptable (Gharieb and Nishikawa, 2021). Pérez-Acebo et al. (2020) developed another MLR model for IRI prediction for flexible pavements in Spain. The developed model provided relatively fair IRI estimation with a coefficient of determination (R^2) of 0.48. Nowadays, soft computing techniques have been widely applied to estimate the IRI of rigid and flexible pavements in different regions. Kaloop et al. (2022) summarized some of these techniques for predicting IRI of rigid pavements. For flexible pavements, Abdelaziz et al. (2020) compared regression and Artificial Neural Networks (ANNs) for the prediction of IRI. Their results concluded that the ANNs outperformed the regression with R^2 of 0.75 and 0.57 for ANNs and regression, respectively. ANN and group method of data handling (GMDH) were compared in predicting IRI, and the results showed that ANN produced more accurate IRI predictions in the short and long terms (Ziari et al., 2016). Adaptive Network based Fuzzy Inference System (ANFIS) as one of developed ANN techniques was found successful in estimating IRI (Terzi, 2013). Genetic algorithm (GA), ANN, and ANFIS methods were proposed by integration with other techniques to improve the estimation of IRI (Nguyen et al., 2019; Mazari and Rodriguez, 2016). ANFIS was integrated with GA, Particle Swarm Optimization (PSO), and the Firefly Algorithm (FA) to improve the performance of ANFIS for IRI prediction of flexible pavements (Nguyen et al., 2019). The PSO-ANFIS yielded better predictions compared to the other models. GA-ANN, ANFIS, ANN, and GA were compared in predicting the IRI of flexible pavements and the GA-ANN yielded more accurate results compared with the other methods (Mazari and Rodriguez, 2016). Machine learning was also employed in calculating pavement condition (Sholevar et al., 2022; Kheirati and Golroo, 2022)

Recently, different hybrid algorithms were widely used in different pavement engineering applications (Kaloop et al., 2019; Karballaeezadeh et al., 2020a,c; Wang et al., 2021; Gabr et al., 2022). PSO-ANN performed well in predicting moduli of flexible pavements (Gopalakrishnan, 2010). On the other hand, Gaussian Process Regression (GPR) and Locally Weighted Polynomials (LWP) were not used yet in predicting IRI of flexible pavements, to the best of the authors knowledge.

GPR and LWP are nonparametric models that were reported to perform well in nonlinear predictions (Rajagopalan and Lall, 1998; Lin et al., 2019; Moore et al., 1997). LWP was efficiently used in modeling a real time hydraulic variable of a salt lake volume, since it exploits the local structure of the function estimation problem(Lall et al., 2006). The GPR performance was found sound in dealing with nonlinear and nonstationary signals (Aye and Heyns, 2017). It was also applied to predict the pan evaporation and its ability in prediction was found acceptable (Shabani et al., 2020). Furthermore, the GPR was compared to hybrid ANN and Support Vector Machine (SVM) to estimate the resilient modulus (M_r) of stabilized base materials (Ghanizadeh et al., 2021). The results showed its preponderance in the prediction compared to other methods. Hu and Solanki (2021) applied the GPR for predicting M_r of cement stabilized subgrade soils and the results indicated very good performance with $R^2 = 0.78$. Karballaeezadeh et al. (2020a,b,c) compared the GPR, M5P model tree, and random forest in modeling the structural number (SN) of flexible pavements and the results showed similar accuracy.

In this consideration, Table 1 summarizes some of the previously developed models for the prediction of IRI and their input parameters, size of database, source of data, goodness of fit metrics and the proposed modeling technique for each model.

As can be seen from the literature models presented in Table 1, some models disregarded initial IRI, which is a very significant parameter in the prediction of IRI as reported in many literature studies (Choi and Do, 2019; Marcelino et al., 2020, 2021; Yamany et al., 2020; Hossain et al., 2019; Ziari et al., 2016; Patrick and Soliman, 2019). Other models used colinear input parameters, such as Jaafar and Fahmi (2016) although they were using the MLR technique in the prediction of IRI which requires all inputs of the model to be independent. Their model used age as well as ESALs which is a function of age. This collinearity may cause overfitting. It should be noted that collinearity of the input parameters is not an issue in machine learning models. As suggested by Jaya et al. (2020) that the best method to overcome the collinearity problem is the use of machine learning techniques, as it has a minimum bias as well as mean squared error of the parameter estimates in addition to minimum residual. Some models achieved excellent goodness of fit, however, the size of the database used for the model development is small and may not cover a wide range of field conditions such as Jaafar and Fahmi (2016), Mazari and Rodriguez (2016), Marcelino et al. (2021), and Yamany et al. (2020). Other models neglected the time or age as a parameter in the IRI prediction such as Marcelino et al. (2020, 2021), and Hossain et al. (2019), while other models disregarded the structure of the pavement, such as Dong et al. (2019), Choi and Do (2019), Yamany et al. (2020), Hossain et al. (2019). Despite some models like Abdelaziz et al. (2020) managed to use distresses which are a function of the pavement structure, material properties, traffic characteristics, and climatic condition in addition to initial IRI (IRI_0) and age, they used combined data from the Long Term Pavement Performance (LTPP) General Pavement Studies (GPS) and the Seasonal Pavement Studies (SPS). While SPS studies were constructed after the launch of LTPP, the GPS sections were constructed long before the initiation of data collection and they do not have any initial IRI measurements. Thus, the authors had to use backcasting to derive initial IRI values.

Therefore, the current research specific objectives are as follows:

1. Estimate the suitable inputs in modeling IRI using regression modeling to assess the sensitivity of several available variables.
2. Examine the robustness of the models using the comprehensive seasonal pavement studies (SPS) of the LTPP database, which unlike the GPS data is confirmed to have initial IRI measurements.
3. Explore new machine learning techniques in predicting IRI of flexible pavements which are the GPR, LWP, PSO-ANN, and PSO-ANFIS.

The selected variables for IRI modeling were used to compare GPR, LWP, PSO-ANN, and PSO-ANFIS. The accuracy of the proposed models was evaluated using different statistical goodness of fit indices.

3. Data collection and methods

3.1. Data collection

Model soundness and credibility depend on the quality of data used for model development. Thus, data was collected from LTPP which contains reliable data covering a wide range of field conditions. Data from SPS flexible pavement sections located in the four different climatic zones in the US was used for models' development and validation.

In this research, datasets belonging to SPS-1 flexible pavement sections with no missing initial IRI data were considered. The number of pavement sections conforming with this criterion was 126 sections containing 925 IRI measurements. The data obtained from the LTPP database includes pavement age, initial IRI and traffic and climate effects on the pavement structure represented by different distresses and their measurements. Following are the details of the variables used in this study. The first important parameter is the initial IRI (IRI_o) which is the IRI measured immediately after construction. This parameter denotes the quality of construction and was reported in many studies to significantly affect the progression of IRI with age (Abdelaziz et al., 2020; ARA, 2008; Mazari and Rodriguez, 2016; Zeiada et al., 2020; Gong et al., 2018; Rifai et al., 2015; Zhou et al., 2021; Guo et al., 2021; Dong et al., 2019; Jaafar and Fahmi, 2016). Other important parameters are the load associated alligator fatigue cracks in the wheel path, longitudinal cracks in the wheel path, rutting, and the

Table 1
Main parameters used for flexible pavements IRI prediction models.

Model	Variables									
	Modeling procedure	IRI_0	Age	Site specific properties		Structural properties	Traffic	Flexible distresses	Data source	Metrics
				Climate	Material properties					
Abdelaziz et al. (2020)	MLR	✓	✓	–	–	–	–	F.C, T.C, SDRUT	LTPP	N = 2439, R^2 = 0.57, S_e/S_y = 0.66
	ANN	✓	✓	–	–	–	–	F.C, T.C, SDRUT	LTPP	N = 2439, R^2 = 0.75
ARA (2008)	MLR	✓	✓	FI, Precip	PI		–	F.C, T.C, RD	LTPP	N = 1926, R^2 = 0.56, SEE = 2.98 m/km
Jaafar and Fahmi (2016)	MLR	✓	✓	–		SN, CN	ESALs	–	LTPP	N = 34, R^2 = 0.26
	ANN	✓	✓	–		SN, CN	ESALs	–	LTPP	N = 34, R^2 = 0.90
Mazari and Rodriguez (2016)	ANN, GEP	✓	✓	–	–	–	ESALs	–	LTPP	N = 98, R^2 = 0.98, RMSE = 0.078 m/km
Zeiada et al. (2020)	ANN	✓	–	RH, AW, FI	MR_{SG} A, E	SCI	ESALs	–	LTTP	N = 115, R^2 = 0.87, MSE = 0.03, RMSE = 0.16, MAE = 0.12
Dong et al. (2019)	LSTM-BPNN	✓	✓	ELE, LAT, LNG + 14 climatic parameters	PM	–	AADTT AADKESAL	PC	LTPP	N = 2243, R^2 = 0.87, RMSE = 0.242
Choi and Do (2019)	RNN	–	–	T, Precip, Deicing	–	–	AADT, ESALs	–	RPM	N = 1880, R^2 = 0.873, RMSE = 0.14
Marcelino et al. (2021)	RFA	–	–	RH, Precip. T, FI,	–	SN, H	AADTT	–	LTPP	N = 27, R^2 = 0.93, AMSE = 0.104
Marcelino et al. (2020)	TLA	–	–	RH, Precip. T, FI,	–	SN, H	AADT	–	LTPP +PRA	N = 2890, R^2 = 0.786
Yamany et al. (2020)	RPR	–	✓	Precip, T, FI	–	–	AADTT. ESALs	–	LTPP	N = 1159, R^2 = 0.48, RMSE = 0.30 m/km
	ANN	–	✓	FI	–	–	–	–	LTPP	N = 1159, R^2 = 0.71 RMSE = 0.26 m/km
Gong et al. (2018)	RFR	✓	✓	Precip, FI			ESALs	F.C, T.C, RD, PT, RV, PSH, PTH	LTPP	N = 11000, R^2 = 0.95 RMSE = 0.26 m/km
Hossain et al. (2019)	ANN	–	–	T, RH, FI, Precip	–	–	ADT, ADTT	–	LTPP	RMSE = 0.027
Ziari et al. (2016)	ANNs	–	✓	T, Precip, FI	–	S_T, H	ESALs, AADT, AADTT	–	LTPP	N = 205, R^2 = 0.95 RMSE = 0.19
Patrick and Soliman (2019)	MLR	–	–	–	–	–	–	F.C, T.C, PT, PTH	LTPP	N = 135, R^2 = 0.75, RMSE = 0.25
Rifai et al. (2015)	DM	✓	✓	–	–	–	ESALs	L.C, RD, PTH	IIRMS	N = 165, R^2 > 0.70
Zhou et al. (2021)	RNN	✓	✓	EVP, Precip, T	–	–	ESALs	RD, F.C, T.C,	LTTP	N = 854, R^2 = 0.93
Guo et al. (2021)	GBDT	✓	✓	Precip	–	H, R_{ac}	ESALs	F.C, T.C, L.C	LTPP	N = 1781, R^2 = 0.90
Alatoom and Al-Suleiman (2021)	ANN	✓	–	–	–	–	ESALs, HV, TV	–	GAM	N = 204, R2 = 0.86, RMSE = 0.37, MAE = 0.10

MLR: Multilinear Regression, ANN: Artificial Neural Network, LSTM-BPNN: Long Short-Term Memory Back Propagation Neural Network, RFA: Random Forest Algorithm, RNN: Recurrent Neural Network, TLA: Transfer Learning Approach, RPs: Random Parameters Regression, RFR: Random Forest Regression, DM: Data Mining, GBDT: Gradient Boosting Decision Tree, IRI_0: Initial IRI, FI = freezing index, Precip: Annual precipitation, T: Temperature, RH: Relative Humidity, AW: Average Wind Velocity, A: Average Albedo, E, Average Emissivity, ELE: Elevation of pavement, LAT: Latitude of pavement, LNG: Longitude of pavement, EVP: Evaporation, MR_{SG}: Resilient modulus of subgrade, PM: Material of pavement, PI: Plasticity Index, SN: Structural Number, CN: Construction Number, SCI: Structural Capacity Index, ST: Surface Thickness, H: Pavement Thickness, R_{ac}: ratio between asphalt thickness and total pavement thickness, T.C: Transverse cracking, F.C: fatigue cracking, SDRUT: standard deviation of rut depth, RD: Rut Depth, PC: Pavement conditions, PT: Patch, RV: Raveling, PSH: Polishing, PTH: Potholes, ESAL: Equivalent Single Axle Loads, AADTT Annual average daily truck traffic, AADKESAL: Annual equivalent single-axle loads, HV: Heavy Vehicles, TV: Traffic Volume, LTPP: Long Term Pavement Performance data base, RPM: Road Pavement Monitoring Data of Korea, PRA: Portuguese Road Administration, IIRMS: Integrated Indonesia Road Management System, Amman Greater Municipality (GAM), N = number of data points, R^2 = Coefficient of Determination, AMSE: Average Mean Squared Error, RMSE: Root Mean Squared error, MAE Mean Absolute error.

non-load associated transverse (thermal) cracks. In the LTPP database, each distress has three severity levels: low, moderate, and high. In this research, all the severities of each distress were summed up to produce one value. These distresses express the pavement performance with age, which is a function of traffic loading characteristics, traffic volume, pavement material properties, construction quality, pavement structural design, environmental properties, and the subgrade strength. In the current study, the age (age after construction, in years), IRI_o (initial IRI, m/km), sum of all severities of alligator fatigue cracking (FC_{all}) expressed as a percentage of wheel path area, sum of all severities of longitudinal cracking (LC_{all}) expressed in units of m/km, sum of all severities of transverse cracking (TC_{all}) expressed in units of m/km, standard deviation of rut depth (SDRUT), in mm, and PI (percent average plasticity index of subgrade soil) are used as the main input parameters for IRI modeling. These parameters have been considered after comprehensive study of the available literature models (Abdelaziz et al., 2020; National Cooperative Highway Research Program (NCHRP 1-37A), 2004). Table 2 summarizes the statistical description of these variables.

3.2. Research methodology and models development

In this research, four machine learning models are proposed and evaluated. PSO-ANN and PSO-ANFIS are hybrid machine learning models and their previous performance in IRI prediction was found promising (Gopalakrishnan, 2010; Nguyen et al., 2019). Furthermore, two prediction models, GPR and LWP, are proposed and evaluated for IRI predictions for the first time, as far as the authors know. Following are the details of the proposed algorithms and models.

3.2.1. PSO-ANN

A combination of PSO and feedforward ANN was designed and proposed in this paper. Basically, after many trials, the proposed ANN comprises three layers that are basically the input, hidden and output layers, as presented in Fig. 1. The main theory and structures of ANN

Table 2
Descriptive statistics of the main variables.

Variables	IRI (m/km)	Age (year)	IRI_o (m/km)	FC_{all} (%)	LC_{all} (m/km)	TC_{all} (m/km)	SDRUT (mm)	Subgrade PI (%)
Maximum	2.56	15.79	1.44	59.92	745.07	707.89	8.00	43.00
Minimum	0.44	0.00	0.47	0.00	0.00	0.00	0.00	0.00
Mean	0.99	6.24	0.82	3.52	44.09	44.23	1.24	8.35
Skewes	1.59	0.33	0.62	3.43	3.17	3.12	3.14	1.12
Kurtosis	3.81	−0.74	−0.17	13.58	10.32	10.23	15.34	0.37

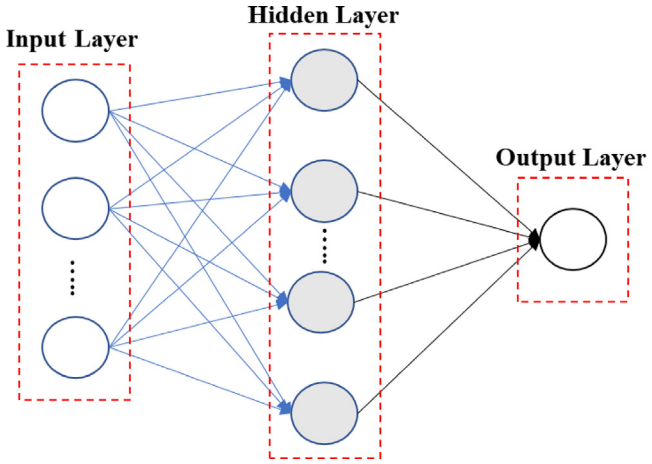

Fig. 1. Structure of feedforward ANN.

can be found in Braspenning et al. (1995), Abdelaziz et al. (2020), Meshram et al. (2020). The layers contain neurons, each neuron output can be expressed as follows (Meshram et al., 2020):

$$O_j = f(\sum_i w_{ij} x_{ij}) \tag{1}$$

where, O_j represents the output of neuron j, f denotes the transfer function, wij are the weight connection between neurons i and j while xij represents the inputs from nodes i to j.

As presented in Eq. (1), the main parameter is the weight. Generally, a trial-and-error method is used to estimate the weight variable. In this study, the PSO was used to find the best solution for the weight. The details of the PSO theory can be found in Marini and Walczak (2015), Nguyen et al. (2019). The PSO begins by producing random swarm particles. Then, the swarm is modernized using the updated position of particles. Consequently, the optimum position of the particles can be obtained by circulating the model processing. The updating process of particles positions can be expressed as follows (Nguyen et al., 2019):

$$v_i^{t+1} = w v_i^t + c_1 r_1 \left(p_{best,i}^t - X_i^t\right) + c_2 r_2 (g_{best,i}^t - X_i^t) \tag{2}$$

$$X_i^{t+1} = X_i^t + v_i^{t+1} \tag{3}$$

where, $X and v$ are the position and speed of the particle, respectively; w is the inertia parameter; and c_1 *and* c_2 denote the cognitive and social component parameters, respectively. r_1 *and* r_2 are randomly assumed in between 0 and 1. $p_{best,i}^t$ *and* $g_{best,i}^t$ are the best positions of the particle at individual and global positions, respectively.

3.2.2. PSO-ANFIS

The PSO-ANFIS is an integration prediction model between PSO and ANFIS algorithms. The proposed model details are presented in Nguyen et al. (2019). A summary of this model can be presented as follows:

The ANFIS is an advance algorithm of ANN; it comprises five layers as shown in Fig. 2 for two inputs as an example. The details of output of each layer can be concluded as by following Eqs. (4) to (8) (Eldessouki and Hassan, 2015):

$$O_i^1 = \begin{cases} \mu_{A_i}(x_1) \\ \mu_{B_i}(x_2) \end{cases} \tag{4}$$

$$O_i^2 = w_i = \mu_{A_i}(x_1) \cdot \mu_{B_i}(x_2) \tag{5}$$

$$O_i^3 = \overline{w_i} = \frac{w_i}{\sum_{j=1}^{N} w_j} \tag{6}$$

$$O_i^4 = \overline{w_i} f_i = \overline{w_i}(p_i x_1 + q_i x_2 + r_i) \tag{7}$$

$$O_i^5 = f = \sum_{i=1}^{N} \overline{w_i} f_i \tag{8}$$

where, O denotes the output of each layer; μ_{A_i} and μ_{B_i} are the membership functions (MF) for x_1 and x_2 inputs, respectively; N is the number of inputs. p_i; q_i and r_i are the parameters of the output function for the i rules calculated through the training process. The weight and normalized weight (w *and* $\overline{w}$, respectively) are calculated in the second and third layers, respectively. As for the PSO-ANFIS, the PSO is used to optimize the best parameters of ANFIS.

3.2.3. LWP

LWP is a nonparametric estimator that works well with heterogeneous and non-stationary datasets (Rajagopalan and Lall, 1998). The main advantage of LWP is its capability of estimator to be expressed as a weighted moving average of the measurements. This is locally defined for each estimated point using a small neighborhood of datasets. Another advantage is the control of the local weights and volume of the neighborhood size for estimation (Lall et al., 2006). The LWP theory for filtering and modeling can be found in Rajagopalan and Lall (1998), Lall et al. (2006), Jekabsons (2016), Lu (1996), Cleveland and Devlin (1988). The LWP was applied in this work for modeling IRI, and it can be summarized as follows (Rajagopalan and Lall, 1998; Lall et al., 2006):

The general regression model can be given as:

$$y_i = f\left(x_i\right) + e_i, i = 1, 2, \ldots .., n \tag{9}$$

where, y *and* x are the response and explanatory variables, respectively, for modeling, f is the transfer function, e is the measurement errors, and n is the number of measurements.

In this research work, a nonlinear transfer function (f) was considered. Thus, Box–Cox family of power transformation was applied to estimate an appropriate transformation. To overcome the calculation complexity in the selection of the best transfer function, Taylor series expansion of $f(x)$ at the estimation point x is commonly used to point out the unknown function (Lall et al., 2006). Taylor uses statistical analysis to recognize a useful generalization Kernel function (weighted moving average = $f(x)$) (Lall et al., 2006). For general background of these concepts, the reader can be referred to the following reference Lall et al. (2006). Here, in general regression by local polynomial solution, a certain number, k, of nearest neighbors of the estimation point x, and to form the $f(x)$ via a locally weighted, polynomial regression over (x, y) data that falls in the neighborhood. Considering the regression relationship between input and output variables in Eq. (9), the LWP assumed the distribution of model error (e) is normal in kth neighborhoods of the estimator points, and that value is ideally zero (Rajagopalan and Lall, 1998; Lall et al., 2006). Thus, the regression

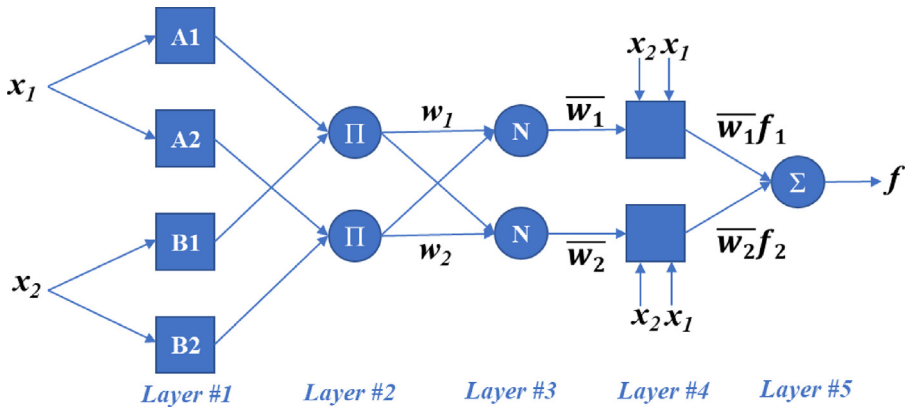

Fig. 2. ANFIS diagram.

function for the local solution of dataset x^* can be considered $y_i = f\left(x_i^*\right), i = 1, 2 \ldots, k$. Therefore, the general setting of transfer function can be expressed as (Lall et al., 2006):

$$f(x) = p_k(x) + f^k(\zeta)\left(x - x_1^*\right) \ldots (x - x_k^*)/k! \tag{10}$$

where, x *and* ζ are the points in the interior of the set of points $\left\{x_1^*, \ldots, x_k^*\right\}$ and $p_k(x) = f[x_1^*, \ldots, x_j^*]$, which defined as the coefficient of the term x^{j-1} of polynomial degree (p) $j-1$.

As presented above, the most significant parameters for finding the best solution of LWP models are k and p. In this work, k was selected based on the kernel bandwidth. The Gaussian kernel in the following equation was applied:

$$K\left(x_0, x\right) = e^{-0.5\left(\frac{\|x - x_0\|}{h(x_0)}\right)^2} \tag{11}$$

where, h is the width of function. For kth determines using the h value, and $h\left(x_0\right) = \left\|x_0 - x_{[k]}\right\|$, where, $x_{[k]}$ is the farthest of the k nearest neighbors x_i to x_0 (Lall et al., 2006).

Further, to select the order of the used function, the data groups were normalized to lie between 0 and 1. Linear, quadratic and cubic orders were used (Lall et al., 2006). Thus, the order was locally selected for kth groups with noting that the $k > 2p$ (Lall et al., 2006). To optimize these parameters, the weighted least square method is used to minimize the model errors:

$$\min_l (y_l - \hat{y}_l)^T w_l (y_l - \hat{y}_l) \tag{12}$$

where, w_l is a $k \times k$ diagonal matrix with elements $w_{ii,l} = K(x_0, x_{j,l}) / \sum_{j=1}^{k} K(x_0, x_{j,l})$. Here, the mean square error was used to determine the best optimization parameters.

3.2.4. GPR

GPR is defined as a nonparametric Bayesian model (Lin et al., 2019; Chen et al., 2020; Kopsiaftis et al., 2019). It directly defines a prior probability distribution over a latent function. This allows it to deal with noisy measurements and solves nonlinear problems (Lin et al., 2019; Al-Juboori and Datta, 2019). However, the GPR computational process increases with the training sample size (Koppel et al., 2021; Terry and Choe, 2021). This issue necessitates approximations for use with streaming data, which mostly lack convergence guarantees (Koppel et al., 2021). The GPR was applied to different civil engineering modeling applications with considering the data limitation (Lin et al., 2019; Chen et al., 2020; Kopsiaftis et al., 2019; Momeni et al., 2020), but as far as the authors know, it was not used for IRI prediction before. In the current study, the data used is limited, 925 IRI measurements, and the GPR can be used in IRI modeling effectively as long as the number of data points is limited. Generally, for modeling the relationship between input and output variables in prior distribution of observed target (y) (as presented in Eq. (9)), the Gaussian distribution with a mean of zero and a variance of σ_n^2, and Gaussian processing (GP) are considered. Thus, Eq. (9) can be rewritten as follows (Lin et al., 2019):

$$y = f(x) \sim N(0, K(x, x) + \sigma_n^2 I_n) \tag{13}$$

where, $K(x, x)$ is a covariance matrix for the training input variables or kernel function. I_n represents identity matrix.

Thus, posterior (predictive) distribution (y^*), under given training dataset **D** and input testing variable x^*, can be expressed as follows (Lin et al., 2019):

$$p\left(y^* | D, x^*\right) \sim N(m\left(y^*\right), K\left(y^*, y^*\right)) \tag{14}$$

The best predicts for y^* are the mean of this distribution, which can be given as follows (Lin et al., 2019):

$$m\left(y^*\right) = K\left(x^*, x\right)\left[K(x, x) + \sigma_n^2 I_n\right]^{-1} y \tag{15}$$

The uncertainty of the prediction value can be presented as follows (Lin et al., 2019):

$$K\left(y^*, y^*\right) = K\left(x^*, x^*\right) - K\left(x^*, x\right)\left[K(x, x) + \sigma_n^2 I_n\right]^{-1} K(x^*, x)^T \tag{16}$$

Fig. 3 demonstrates the GPR process. x *and* x^* represent the input variables of the training and testing phases, respectively. y *and* y^* are the target values in the training and testing phases, respectively. The implicit functions $f(x)$ are totally associated, and each association represents a connection between two hidden variables which are described by the covariance function (Lin et al., 2019).

3.2.5. Assessment of the proposed models' accuracy

To assess the proposed models' accuracy, the mean-absolute-error (MAE), maximum-absolute-error (XAE), root-mean-square-error (RMSE), percentages of RMSE (PE), coefficient of determination (R^2) and Pearson's correlation (R) were employed. In addition, Akaike's information criterion (AIC) was also used to select the best performing model. The following equations present these indices (Gabr et al., 2022; Kaloop et al., 2022):

$$MAE = \frac{1}{n}\sum_{i=1}^{n} |IRI_{ip} - \mathrm{IRI}_{im}| \tag{17}$$

$$XAE = \max_i\left(\left|IRI_{ip} - \mathrm{IRI}_{im}\right|\right) \tag{18}$$

$$RMSE = \sqrt{\frac{\sum_{i=1}^{n}(IRI_{ip} - \mathrm{IRI}_{im})^2}{n}} \tag{19}$$

$$PE = \frac{RMSE \times 100}{IRI_{max} - \mathrm{IRI}_{min}} \tag{20}$$

$$R^2 = \left(1 - \frac{\sum_{i=1}^{n}\left(\mathrm{IRI}_{ip} - \overline{\mathrm{IRI}}\right)^2}{\sum_{i=1}^{n}\left(\mathrm{IRI}_{im} - \overline{\mathrm{IRI}}\right)^2}\right) \tag{21}$$

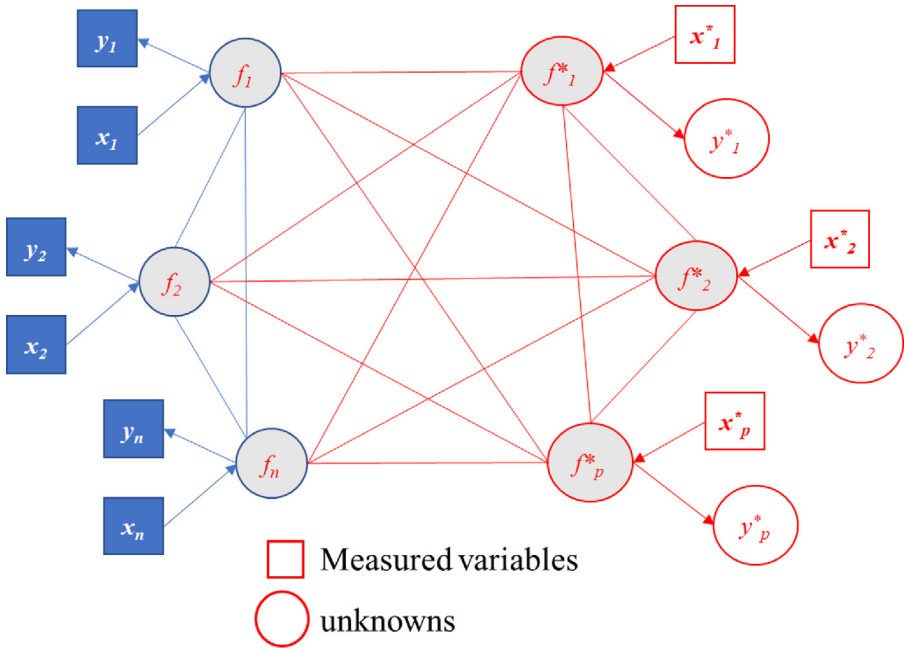

Fig. 3. GPR processing diagram.

$$R = \left(\frac{COV\left(IRI_m, \mathrm{IRI}_p\right)}{\sigma_{\mathrm{IRI}_m}\sigma_{\mathrm{IRI}_p}}\right) \tag{22}$$

$$AIC = n\ln\left(\frac{1}{n}\sum_{i=1}^{n}\left(IRI_{ip} - \mathrm{IRI}_{io}\right)^2/n\right) + 2p \tag{23}$$

where, $IRI_{ip}, \mathrm{IRI}_{im}$, *and* $\overline{\mathrm{IRI}}$ are the predicted, measured and mean of IRI values, respectively; IRI_{max} and IRI_{min} are the maximum and minimum measured IRI, respectively; n is the number of data points, $COV(IRI_m, \mathrm{IRI}_p)$ is the covariance between measured and predicted IRI, and σ_{IRI_m} and σ_{IRI_p} are the standard deviation of the measured and predicted IRI, respectively.

4. Results and discussion

4.1. Development of the IRI predictive models

Four multi-input single-output (MISO) machine learning prediction models are proposed in this paper. The data presented in section 2.1 was used and first classified using the regression technique, as presented in the results section. From the regression results evaluation, seven variables were found to have significant influence on IRI. These variables which were also confirmed by other researchers to significantly affect the IRI are age, IRI_o, AC_{all}, FC_{all}, TC_{all}, SDRUT and PI (Abdelaziz et al., 2020; ARA, 2008). These variables were used to develop the MISO machine learning models. The 925 IRI measurements were divided into training (70%) and testing (30%) to design and validate the proposed models. Fig. 4 shows the linear correlation matrix between the selected variables for the whole dataset (Abdelaziz et al., 2020). In addition, Fig. 5 presents the histogram of the input and output variables. The relationship between normal distribution of the input and output variables is also presented in Fig. 5. From Fig. 4, it can be concluded that the correlation between IRI and each input variable ranges from very weak for the PI to significant for IRI_o. In addition, the statistical data shown in Table 2 and data distribution in Fig. 5 show that the distribution of datasets is not normal. The normal distributions of each input with output variables are not correlated. These results indicate that the relationship between IRI and most of the selected variables is nonlinear. This finding increases the complexity of the design of an effective and accurate prediction model.

Therefore, the proposed models in the current study were designed based on the regression classification. The selected data was first normalized to fall between 0 to 1 in order to overcome the different ranges of input variables. The seven variables were used as inputs while IRI is the output for the MISO models. The PSO-ANFIS and PSO-ANN were employed to compare their performance with the newly proposed GPR and LWP techniques for IRI prediction. The design parameters of the PSO-ANN model are the hidden neurons numbers, c_1, c_2, w and population number. In the current work, the optimum number of hidden neurons was found to be four based on the trial-and-error technique and using the MSE for optimizing the best fitting values. The PSO c_1 *and* c_2 were set to 1.5 and 2.5, respectively. The value of "w" was initially set to 0.1 and random incremental coefficient was utilized. The r_1 and r_2 values were 0.267. To optimize the particles (population) numbers, the trial-and-error was applied to detect the number of the best particles, which was found to be 10.

In developing the PSO-ANFIS model, as the same for PSO-ANN, w, population number, $c_1$andc_2 should be optimized to achieve the minimum MSE. The best values were found to be 0.4, 25, 1 and 2, respectively. In LWP, the transfer function, width (h), and function order are the main parameters for the model. In the current work, the best function was the Gaussian function with h = 15.82 and three orders. Furthermore, the trial-and-error was applied to optimize the GPR model. Here, we used the mean function for m(x) and covariance matrix is a kernel function defined on the input's variables. The final parameters obtained for IRI prediction are the squared exponential kernel function with a separate length scale per predictor in which the mean and standard deviation were equal to zero and 0.145, respectively. Herein, different kernel functions were evaluated, and the best performance of the proposed model was obtained when using the squared exponential kernel function. Furthermore, the exact prediction and fitting methods were used, and the basis function was constant. The weight of each of the GPR input variables model was estimated as shown in Fig. 6(a). From the figure, the IRI_o, with weight = 0.99, has a full contribution in modeling IRI followed the PI, while the contributions of FC_{all}, LC_{all}, TC_{all}, SDRUT were noticed to be very small, as their weights were close to zero. Moreover, to evaluate the proposed GPR model, the performance of the model prediction in the testing stage was statistically evaluated and presented in Fig. 6(b).

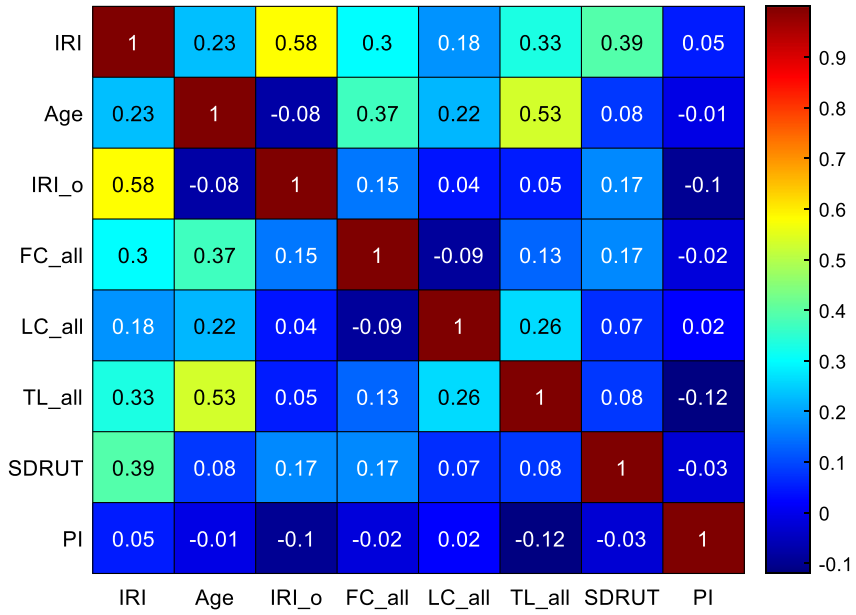

Fig. 4. Variable's correlation matrix.

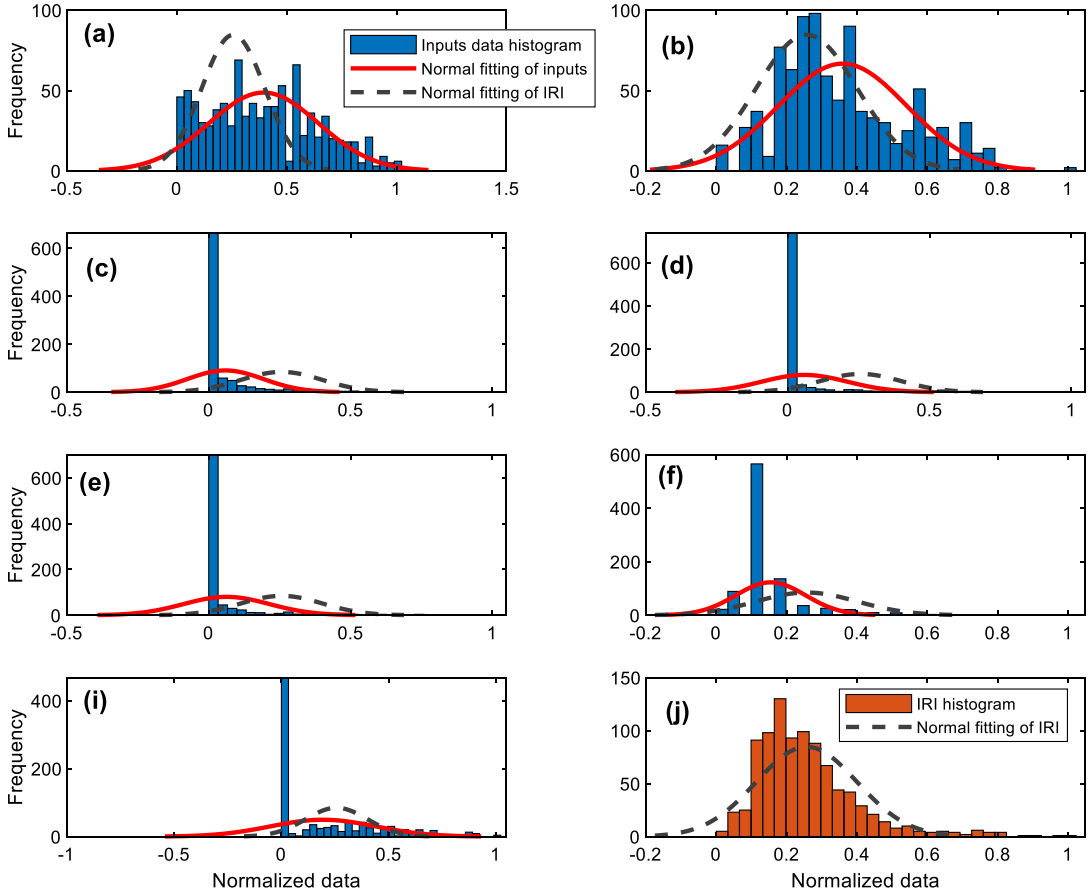

Fig. 5. Input and output variables distributions, (a) Age, (b) IRI_o, (c) FC_{all}, (d) LC_{all}, (e) TC_{all}, (f) SDRUT, (i) PI, (j) IRI.

The predicted IRI values in the testing stage fall within the ±95% confidence interval. This means that the GPR model can be used to accurately estimate IRI. The MATLAB software was used to develop and implement the proposed models, and the code is available as a supplementary material (The Mathworks Inc., 2016).

4.2. Data classification and selection

First, the MLR was used to classify the collected LTPP dataset and to estimate the significant variables that can be used in modeling IRI of flexible pavements. The MLR is commonly used in pavement

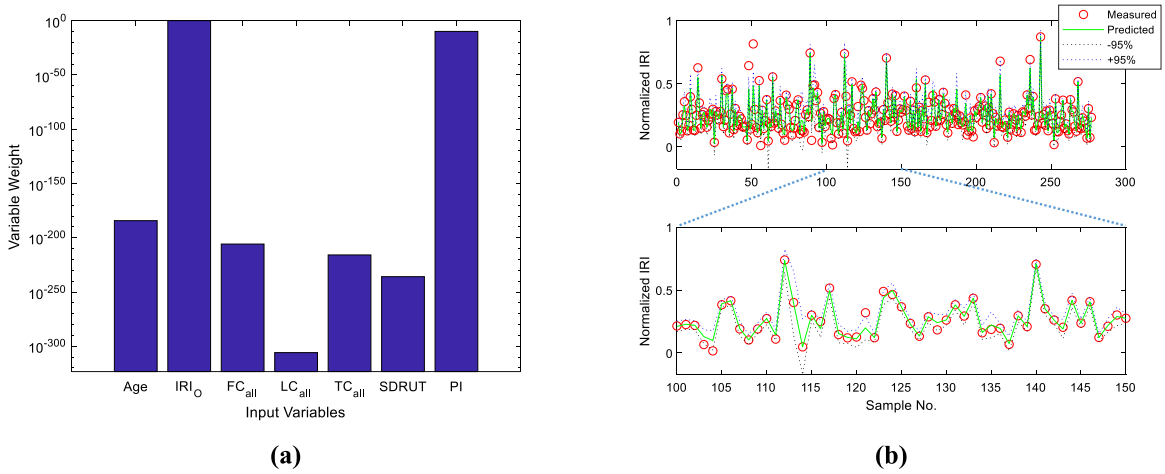

Fig. 6. GPR model performance, (a) predictor weight, (b) confidence interval of predicted IRI in the testing stage.

characteristics determination (Abd El-Hakim and El-Badawy, 2013; Abdelaziz et al., 2020; Gabr et al., 2022). From the previous studies, the pavement age, IRIo, distresses and climate effects, soil parameters, and traffic and structural parameters are usually used in modeling IRI of pavements (Abdelaziz et al., 2020). Pavement age and IRI_o were reported to be more efficient than other variables in modeling IRI of flexible pavements (Abdelaziz et al., 2020). Fig. 7 shows the best MLR model obtained from the conducted trials. Eq. (24) represents the relation between the inputs and IRI. The best model inputs include $IRI_O, Age, FC_{all}, LC_{all}, TC_{all}, SDRUT, PI$. This model yielded the best performance in IRI modeling of flexible pavements with R^2 of 0.528 which agrees with other literature studies [2], (Abd El-Hakim and El-Badawy, 2013; ARA, 2008). However, this model still shows high scatter and bias in predictions as depicted in Fig. 7. Therefore, machine learning models were proposed to evaluate their performance against the MLR using the same variables.

$$IRI = IRI_O + 0.37\times10^{-3}Age + 5.38\times10^{-3}FC_{all} + 0.20\times10^{-3}LC_{all} + 0.69\times10^{-3}TC_{all} + 72.54\times10^{-3}SDRUT + 3.20\times10^{-3}PI \quad (24)$$

4.3. Proposed models evaluation

Table 3 presents the performance of the proposed models in terms of different goodness of fit statistics. In addition, Fig. 8 illustrates the relationship between measured and predicted IRI in the testing phase. The high R and R^2 values indicate good correlation between measured and predicted IRI, while the low values of RMSE, MAE, XAE, PE and AIC denote low model errors. The highest correlation and lowest error indicate the best performing and more accurate model. Table 3 shows that the performance of the GPR and LWP is better compared to PSO-ANFIS and PSO-ANN models. In addition, the AIC values indicate that the AIC of the GPR model is low in the training and testing stages, followed by the LWP model. While the inferior model is the PSO-ANN with AIC = 136.257 and high RMSE = 0.189 m/km. Moreover, the correlation between measured and predicted IRI in the testing stage presented in Fig. 8 shows that the performance of the GPR model is the best among the proposed models. However, the correlation between best fit and linear fitting of the datasets demonstrates that the LWP has the lowest bias. The GPR modeling technique was found superior compared to the other investigated techniques with PE = 0.004% and 3.98% for the training and testing stages, respectively. Herein, the rank analysis of the statistical indices of the proposed models concludes that the GPR model can be accurately used in IRI prediction of the flexible pavements.

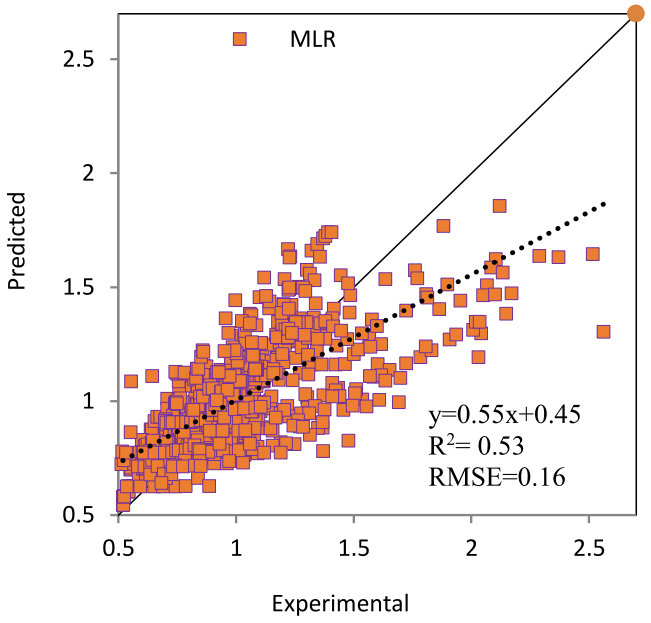

Fig. 7. Best MLR model in predicting IRI of flexible pavement.

The presented Taylor and Violin plots in Fig. 9 illustrate the overall evaluation of the proposed models in the testing stage. Taylor plot presents in one diagram the model standard deviation in x- and y-axes while the blue dotted lines demonstrate these values. The black dashed lines show the correlation coefficients of the proposed models with measured values. RMSE is presented in dotted pink lines. The best model is the one closer to the x-axis with zero standard deviation and low RMSE. From Fig. 9(a), it can be concluded that the GPR is the best performing model based on the explained evaluation criterion, followed by the LWP model. On the other hand, the Violin plot (Fig. 9(b)). graphically presents the model's errors in the testing stage. Even though most of the models showed very close mean and median error values, the GPR showed the lowest variation in the model error followed by LWP, while the PSO-ANN model showed the largest variation in the model error. In addition, the median and mean of GPR and LWP models are almost equal. This means that the model errors in the testing stage follow the normal distribution. These results indicate that the GPR and LWP models can accurately predict the IRI of flexible pavements.

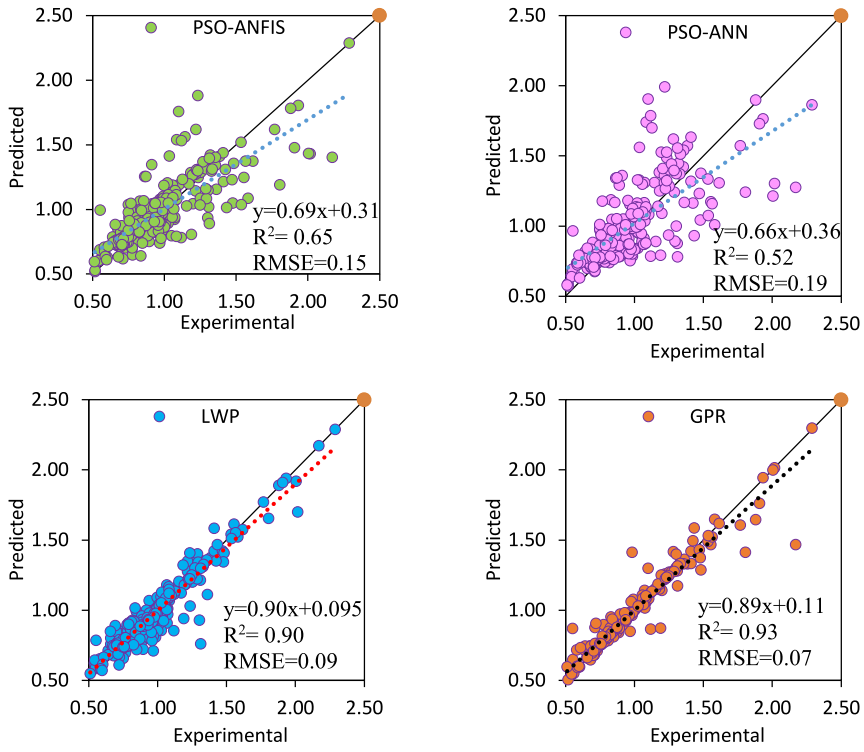

Fig. 8. Proposed models performances in the testing phase.

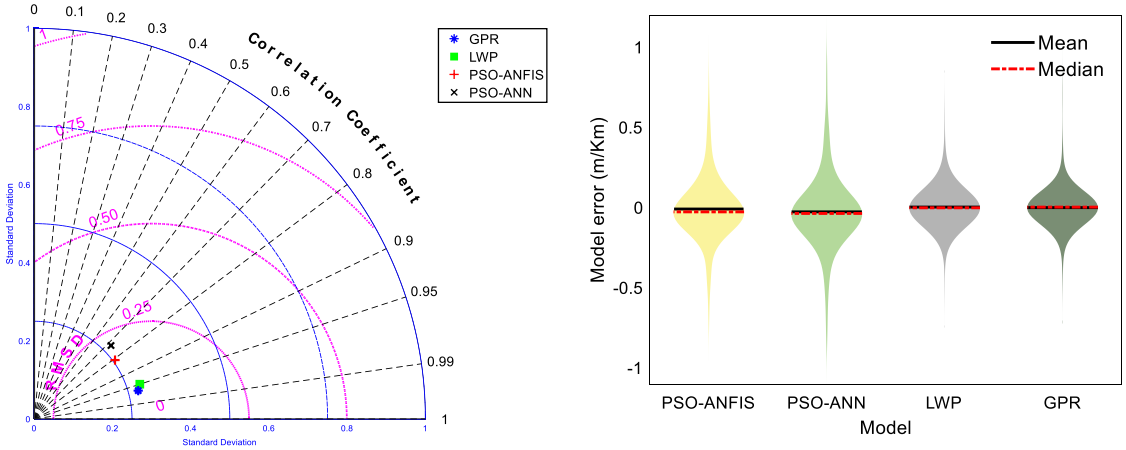

(a) Taylor diagram (b) Violin plot

Fig. 9. Visualizing of the overall accuracy of the proposed models in the testing stage.

Table 3 and Fig. 9 show that the GPR outperforms all proposed IRI models.

For more in-depth investigation, the whole dataset was used and evaluated in modeling IRI using MLR, GPR, LWP, PSO-ANN, and PSO-ANFIS. Fig. 10 presents the scatter plots of the proposed models. Furthermore, Fig. 7 presents the performance of the MLR model. The correlation between measured and predicted IRI shows that the R values of the MLR, GPR, LWP, PSO-ANN, and PSO-ANFIS are 0.73, 0.99, 0.91, 0.78, and 0.83, respectively. In addition, the correlation between best fitting and linear fitting of the data used is higher for the GPR model compared to the other models, as outlined in Fig. 10. The RMSE of model's errors are 0.16 m/km, 0.04 m/km, 0.12 m/km, 0.16 m/km, and 0.14 m/km for the MLR, GPR, LWP, PSO-ANN, and PSO-ANFIS, respectively. The lowest RMSE was found for the GPR model. Herein, the computational time of the GPR and LWP models is computed, and the results showed that the time processing for the whole datasets is 7 and 7.5 s, respectively.

Moreover, the distribution of the models' errors is delineated in Fig. 11. The mean and standard deviation of the GPR model error are −0.0010394 m/km and 0.04362 m/km, respectively. One can surmise that the mean is very close to zero with a very low standard deviation meaning accurate model predictions. For the LWP model errors, the

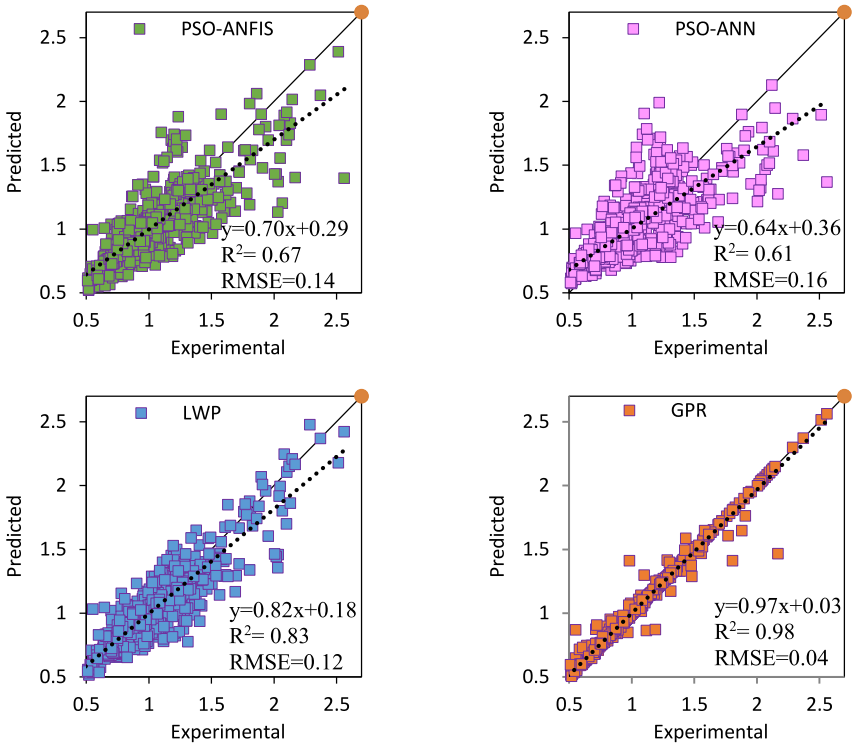

Fig. 10. Proposed models performances for the whole data.

Table 3
Data changes in parametric analysis.

Input variables		No. of data input	Variables at constant value
Parameter	Normalized range		
Age	0–0.9	10	IRI_o, FC_{all}, LC_{all}, TC_{all}, SDRUT, PI
IRI_o	0–0.9	10	Age, FC_{all}, LC_{all}, TC_{all}, SDRUT, PI
FC_{all}	0–0.9	10	Age, IRI_o, FC_{all}, TC_{all}, SDRUT, PI
LC_{all}	0–0.9	10	Age, IRI_o, FC_{all}, TC_{all}, SDRUT, PI
TC_{all}	0–0.9	10	Age, IRI_o, FC_{all}, LC_{all}, SDRUT, PI
SDRUT	0–0.9	10	Age, IRI_o, FC_{all}, LC_{all}, TC_{all}, PI
PI	0–0.9	10	Age, IRI_o, FC_{all}, LC_{all}, TC_{all}, SDRUT

mean and standard deviation are −2.8224e−12 m/km and 0.12944 m/km, respectively. The mean of errors is −0.0077522 m/km and standard deviation of error is 0.19334 m/km for the PSO-ANN model. For the PSO-ANFIS model, the mean = −0.0014705 m/km and standard deviation= 0.16809 m/km. Meanwhile, for the MLR model, the mean = −0.010635 m/km and standard deviation= 0.20626 m/km. From Fig. 11, it can be discerned that the errors of the proposed models follow the normal distribution. This means that the proposed models can be accurately used in IRI prediction with the highest accuracy for the GPR model.

For more investigation on the overfitting problem, a different dataset was used for formulating the GPR model. A simulated dataset was created as shown in Table 4. The impact of each parameter was evaluated while keeping other parameters as a constant. In other words, one input variable was changed linearly at a time to generate IRI predictions, while all other variables were kept constant at their mean values. The results of the parametric analysis are presented in Fig. 12.

From Fig. 12, it can be observed that an increase in all variables except PI yielded a corresponding increase in IRI which was also reported in the study of (Abdelaziz et al., 2020). Hence, the parametric evaluation captured the same trend of IRI with varying Age, FCall, LCall, TCall, and SDRUT. However, the change in FC_{all}, LC_{all}, TC_{all}, and SDRUT from 0–0.9 only affects IRI with a range of 4.3e−5, 3.4e−9, 5.4e−4, and 0.013, respectively. This indicates that the influences of these parameters are small in estimating IRI values. In contrast, the change of Age, IRI_o and PI from 0–0.9 affects the predicted IRI with a change of about 0.11, 0.63 and 0.15, respectively. This implies the importance of IRIo, PI, and Age, respectively as predictors of IRI which agree with the results of (Abdelaziz et al., 2020). Finally, IRI was observed to have a complex 5- and 4-degrees polynomial with changes of IRI_o and PI, respectively. This indicates that the GPR model is rational and valid even with the simplifications used to estimate IRI through complex input variables.

The goal of this study was to use the GPR and LWP for IRI prediction of flexible pavement as new techniques and compare them to some existing hybrid models. Details of previous models and their accuracy were also provided. Thus, the main advantages of nonparametric models, GPR and LEP, include (a) faster computation (less than 8 s), (b) lower computational cost, and (c) higher generalization ability and

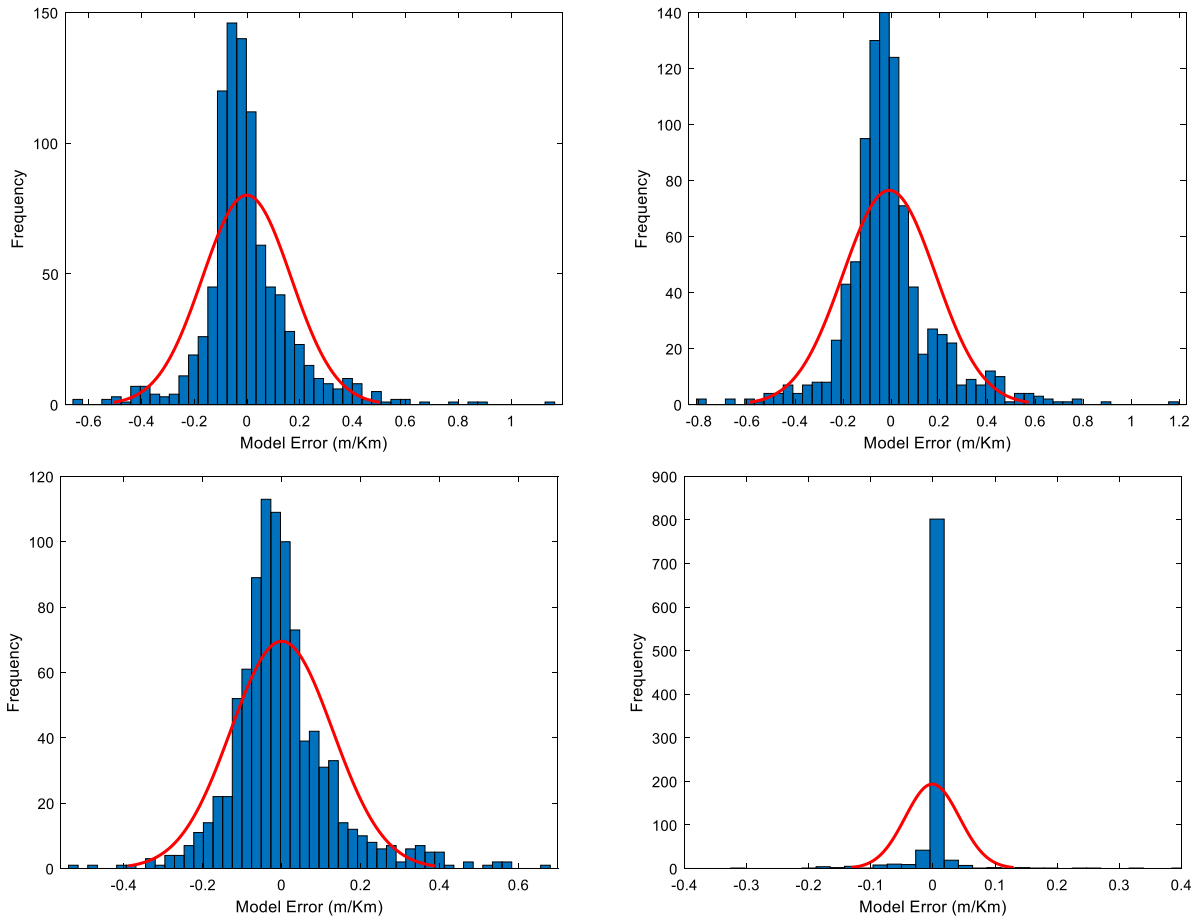

Fig. 11. Models' errors histogram and normal fitting, red line, for (a) PSO-ANFIS, (b) PSO-ANN, (c) LWP, (d) GPR.

accuracy (based on this study results). However, the optimum developed models can predict an accurate IRI values that ranged between the data used and data numbers. Therefore, further research should be implemented to ensure the robustness if out-of-range data is used. The future direction of this study may include (i) a comprehensive assessment of the accuracy of GPR using other datasets from different fields with increased database; (ii) a comparative assessment of hybrid and conventional GPR methods for improving the complexity of GPR in modeling with stream datasets; and (iii) a comparative assessment of nonparametric models with another group of optimization algorithms (OAs), such as evolutionary and physics-based OAs.

5. Conclusions

A total of 925 IRI measurements representing 126 SPS-1 sections from the LTPP located in different US climate zones were collected, classified, and used for IRI modeling. The MLR classification of the collected datasets showed that pavement age, initial IRI, alligator, longitudinal and transverse cracking, plasticity index of subgrade soil and standard deviation of rut depth are the main input variables affecting flexible pavement IRI modeling. Two new soft computing models for flexible pavement performance using IRI were developed in this work which are the GPR and LWP. These models' performance was evaluated and compared with MLR, PSO-ANN and PSO-ANFIS. Based on the analyses of the presented results the following conclusions can be drawn:

- The comparative evaluation of GPR, LWP and MLR, PSO-ANN and PSO-ANFIS models showed that the GPR and LWP models for IRI prediction of flexible pavements are more accurate.
- Comparing GPR and LWP showed the robustness and consistency of the GPR model in correlation and error evaluation.
- The correlation between measured and predicted IRI showed that the R^2 of the GPR and LWP were 0.93 and 0.90, respectively while the RMSE values were 0.04 m/km and 0.12 m/km for GPR and LWP, respectively.
- The GPR can be used accurately and effectively for modeling IRI of flexible pavements with a model error of only 3.98% and lower computational time.

The proposed method is a simple and direct method that can be used by researchers as well as practitioners to effectively predict the IRI of flexible pavements to be used in pavement management systems. An algorithm representing the GPR model is added in Appendix A. This simple algorithm can be implemented in the Pavement ME Design guide or a similar method to predict IRI of flexible pavements. This will facilitate the designers' job to precisely predict flexible pavement IRI using simple software, and entitle them to estimate the future maintenance requirements, hence assigning future fund needs required to maintain pavement condition, enhance its function, and prolong its service life. Moreover, for pavement designers, estimated IRI at the end of pavement service life could be used as a single standard of design when compared to the pre-estimated terminal IRI. While for contractors and DOTs, this software can be used to estimate IRI values to reward or inflict a penalty on contractors based on the quality of the constructed pavement. Finally, this model can be used by DOTs or highway authorities to calculate IRI from measured distresses in cases where no IRI measurement equipment is available. This can be achieved both on a project level or on a network level.

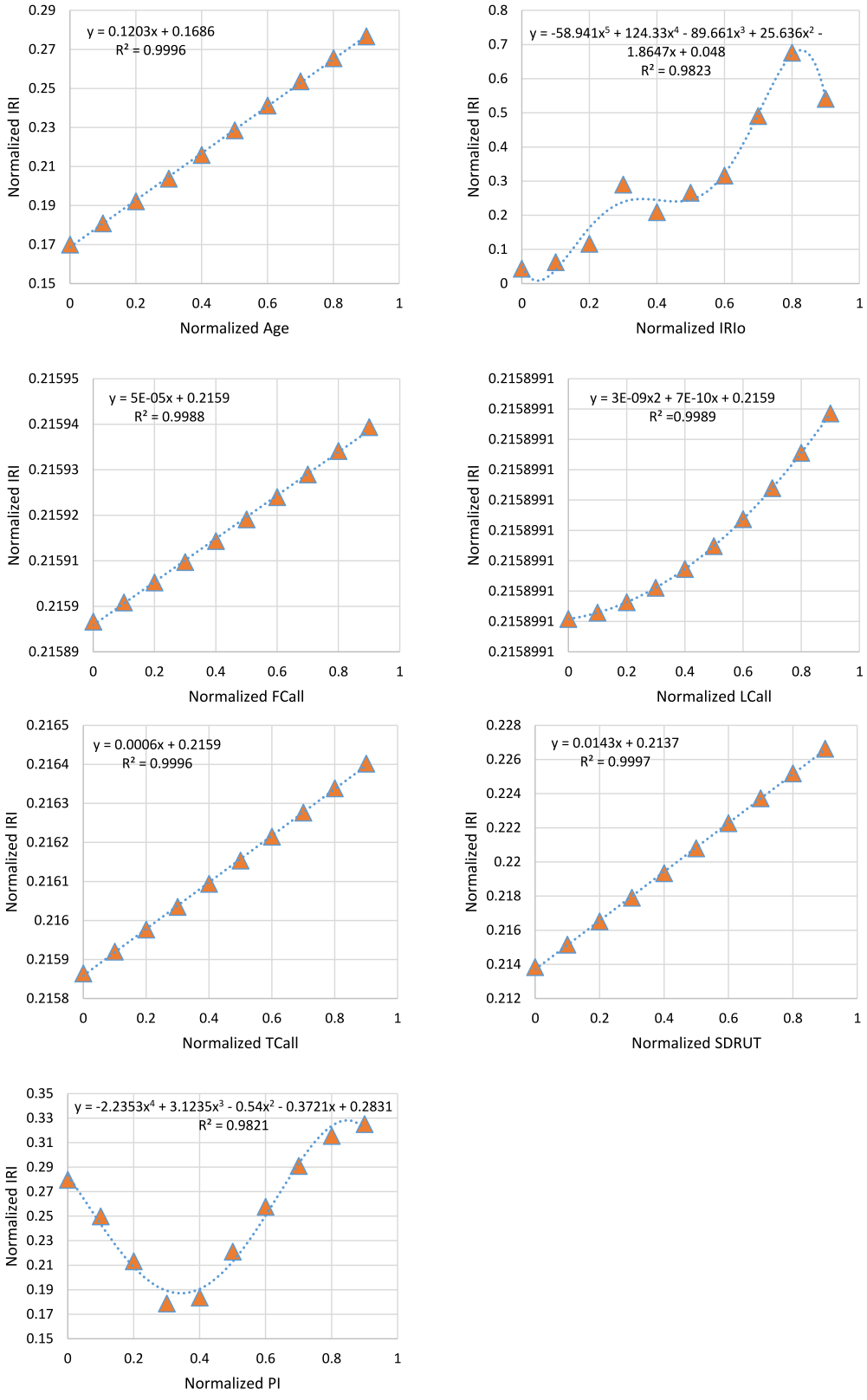

Fig. 12. Parametric study of the developed GPR model.

CRediT authorship contribution statement

Mosbeh R. Kaloop: Conceptualization, Methodology, Formal analysis, Investigation, Data curation, Software, Validation, Visualization, Writing – original draft. **Sherif M. El-Badawy:** Conceptualization, Investigation, Validation, Supervision, Data curation, Visualization, Writing – review & editing. **Jong Wan Hu:** Visualization, Supervision, Funding acquisition, Project administration. **Ragaa T. Abd El-Hakim:** Conceptualization, Methodology, Formal analysis, Investigation, Data curation, Visualization, Writing – original draft.

Declaration of competing interest

The authors declare that they have no known competing financial interests or personal relationships that could have appeared to influence the work reported in this paper.

Data availability

No data was used for the research described in the article.

Acknowledgment

This work was supported by the National Research Foundation of Korea (NRF) grant funded by the Korean government (MSIT) (NRF-2021R1A2B5B02002599).

Appendix A

The GPR MATLAB live script is available in the supplementary materials.

Appendix B. Supplementary data

Supplementary material related to this article can be found online at https://doi.org/10.1016/j.engappai.2023.106007.

References

Abd El-Hakim, Ragaa, El-Badawy, Sherif, 2013. International roughness index prediction for rigid pavements: An Artificial Neural Network application. Adv. Mater. Res. 723 (August), 854–860. http://dx.doi.org/10.4028/www.scientific.net/AMR.723.854.

Abdelaziz, Nader, El-Hakim, Ragaa T. Abd, El-Badawy, Sherif M., Afify, Hafez A., 2020. International roughness index prediction model for flexible pavements. Int. J. Pav. Eng. 21 (1), 88–99. http://dx.doi.org/10.1080/10298436.2018.1441414.

Al-Juboori, Muqdad, Datta, Bithin, 2019. Optimum design of hydraulic water retaining structures incorporating uncertainty in estimating heterogeneous hydraulic conductivity utilizing stochastic ensemble surrogate models within a multi-objective multi-realisation optimisation model. J. Comput. Des. Eng. 6 (3), 296–315. http://dx.doi.org/10.1016/j.jcde.2018.12.003.

Alatoom, Yazan Ibrahim, Al-Suleiman, Turki I., 2021. Development of pavement roughness models using Artificial Neural Network (ANN). Int. J. Pav. Eng. 1–16. http://dx.doi.org/10.1080/10298436.2021.1968396.

ARA, 2008. A Manual of Practice.

Aye, S.A., Heyns, P.S., 2017. An integrated Gaussian process regression for prediction of remaining useful life of slow speed bearings based on acoustic emission. Mech. Syst. Signal Process. 84 (February), 485–498. http://dx.doi.org/10.1016/j.ymssp.2016.07.039.

Braspenning, P.J., Thuijsman, F., Weijters, A., 1995. Artificial Neural Networks: An Introduction to ANN Theory and Practice. Psicothema.

Chen, Zexun, Wang, Bo, Gorban, Alexander N., 2020. Multivariate Gaussian and student-T process regression for multi-output prediction. Neural Comput. Appl. 32 (8), 3005–3028. http://dx.doi.org/10.1007/s00521-019-04687-8.

Choi, Seunghyun, Do, Myungsik, 2019. Development of the road pavement deterioration model based on the deep learning method. Electronics 9 (1), 3. http://dx.doi.org/10.3390/electronics9010003.

Cleveland, William S., Devlin, Susan J., 1988. Locally weighted regression: An approach to regression analysis by local fitting. J. Amer. Statist. Assoc. 83 (403), 596–610. http://dx.doi.org/10.1080/01621459.1988.10478639.

Dong, Yushun, Li, Sili, Shao, Yingxia, Quan, Lei, Du, Junping, Li, Xiaotong, Zhang, Wei, 2019. Forecasting pavement performance with a feature fusion LSTM-BPNN model. In: International Conference on Information and Knowledge Management, Proceedings. http://dx.doi.org/10.1145/3357384.3357867.

Eldessouki, Mohamed, Hassan, Mounir, 2015. Adaptive neuro-fuzzy system for quantitative evaluation of woven fabrics' pilling resistance. Expert Syst. Appl. 42 (4), 2098–2113. http://dx.doi.org/10.1016/j.eswa.2014.10.013.

Elhadidy, Amr A., El-Badawy, Sherif M., Elbeltagi, Emad E., 2021. A simplified pavement condition index regression model for pavement evaluation. Int. J. Pav. Eng. 22 (5), 643–652. http://dx.doi.org/10.1080/10298436.2019.1633579.

Gabr, Alaa R., Roy, Bishwajit, Kaloop, Mosbeh R., Kumar, Deepak, Arisha, Ali, Shiha, Mohamed, Shwally, Sayed, Hu, Jong Wan, El-Badawy, Sherif M., 2022. A novel approach for resilient modulus prediction using extreme learning machine-equilibrium optimiser techniques. Int. J. Pav. Eng. 23 (10), 3346–3356. http://dx.doi.org/10.1080/10298436.2021.1892109.

Ghanizadeh, Ali Reza, Heidarabadizadeh, Nasrin, Heravi, Fahimeh, 2021. Gaussian process regression (GPR) for auto-estimation of resilient modulus of stabilized base materials. J. Soft Comput. Civ. Eng. 5 (1), 80–94.

Gharieb, Mohamed, Nishikawa, Takafumi, 2021. Development of roughness prediction models for Laos National Road Network. CivilEng 2 (1), 158–173. http://dx.doi.org/10.3390/civileng2010009.

Gong, Hongren, Sun, Yiren, Shu, Xiang, Huang, Baoshan, 2018. Use of random forests regression for predicting IRI of asphalt pavements. Construct. Build. Mater. 189 (November), 890–897. http://dx.doi.org/10.1016/j.conbuildmat.2018.09.017.

Gopalakrishnan, Kasthurirangan, 2010. Neural network–swarm intelligence hybrid nonlinear optimization algorithm for pavement moduli back-calculation. J. Transp. Eng. 136 (6), 528–536. http://dx.doi.org/10.1061/(ASCE)TE.1943-5436.0000128.

Guo, Runhua, Fu, Donglei, Sollazzo, Giuseppe, 2021. An ensemble learning model for asphalt pavement performance prediction based on gradient boosting decision tree. Int. J. Pav. Eng. April, 1–14. http://dx.doi.org/10.1080/10298436.2021.1910825.

Hossain, M.I., Gopisetti, L.S.P., Miah, M.S., 2019. International roughness index prediction of flexible pavements using neural networks. J. Transp. Eng. Part B: Pavements 145 (1), 04018058. http://dx.doi.org/10.1061/JPEODX.0000088.

Hu, Xi, Solanki, Pranshoo, 2021. Predicting resilient modulus of cementitiously stabilized subgrade soils using neural network, support vector machine, and Gaussian process regression. Int. J. Geomech. 21 (6), 04021073. http://dx.doi.org/10.1061/(ASCE)GM.1943-5622.0002029.

Jaafar, Mohamed, Fahmi, Zul, 2016. Asphalt pavement roughness modeling using the Artificial Neural Network and linear regression approaches for LTPP southern region. In: Transportation Research Board 95th Annual Meeting (No. 16-4191). Paper Numbers: 16-4191.

Jaya, I. Gede Nyoman Mindra, Ruchjana, Budi Nurani, Abdulah, Atje Setiawan, 2020. Comparison of different Bayesian and machine learning methods in handling multicollinearity problem: A Monte Carlo simulation study. ARPN J. Eng. Appl. Sci. 15 (18), 1998–2011.

Jekabsons, G., 2016. Locally Weighted Polynomials Toolbox for Matlab/Octave. Riga Technical University, 2016, http://www.cs.rtu.lv/jekabsons/regression.html.

Kaloop, Mosbeh R., El-Badawy, Sherif M., Ahn, Jungkyu, Sim, Hyoung-Bo, Hu, Jong Wan, El-Hakim, Ragaa T. Abd El-Hakim, 2022. A hybrid wavelet-optimally-pruned extreme learning machine model for the estimation of international roughness index of rigid pavements. Int. J. Pav. Eng. 23 (3), 862–876. http://dx.doi.org/10.1080/10298436.2020.1776281.

Kaloop, Mosbeh R., Kumar, Deepak, Samui, Pijush, Gabr, Alaa R., Hu, Jong Wan, Jin, Xinghan, Roy, Bishwajit, 2019. Particle swarm optimization algorithm-extreme learning machine (PSO-ELM) model for predicting resilient modulus of stabilized aggregate bases. Appl. Sci. 9 (16), 3221. http://dx.doi.org/10.3390/app9163221.

Karballaeezadeh, Nader, S., Danial Mohammadzadeh, Moazemi, Dariush, Band, Shahab S., Mosavi, Amir, Reuter, Uwe, 2020a. Smart structural health monitoring of flexible pavements using machine learning methods. Coatings 10 (11), 1100. http://dx.doi.org/10.3390/coatings10111100.

Karballaeezadeh, Nader, Tehrani, Hosein Ghasemzadeh, Shadmehri, Danial Mohammadzadeh, Shamshirband, Shahaboddin, 2020b. Estimation of flexible pavement structural capacity using machine learning techniques. Front. Struct. Civ. Eng. 14 (5), 1083–1096. http://dx.doi.org/10.1007/s11709-020-0654-z.

Karballaeezadeh, Nader, Zaremotekhases, Farah, Shamshirband, Shahaboddin, Mosavi, Amir, Nabipour, Narjes, Csiba, Peter, Várkonyi-Kóczy, Annamária R., 2020c. Intelligent road inspection with advanced machine learning; Hybrid prediction models for smart mobility and transportation maintenance systems. Energies 13 (7), 1718. http://dx.doi.org/10.3390/en13071718.

Kheirati, Afarin, Golroo, Amir, 2022. Machine learning for developing a pavement condition index. Autom. Constr. 139 (March), 104296. http://dx.doi.org/10.1016/j.autcon.2022.104296.

Koppel, Alec, Pradhan, Hrusikesha, Rajawat, Ketan, 2021. Consistent online Gaussian process regression without the sample complexity bottleneck. Stat. Comput. 31 (6), 76. http://dx.doi.org/10.1007/s11222-021-10051-5.

Kopsiaftis, George, Protopapadakis, Eftychios, Voulodimos, Athanasios, Doulamis, Nikolaos, Mantoglou, Aristotelis, 2019. Gaussian process regression tuned by Bayesian optimization for seawater intrusion prediction. Comput. Intell. Neurosci. 2019 (January), 1–12. http://dx.doi.org/10.1155/2019/2859429.

Lall, Upmanu, Moon, Young-Il, Kwon, Hyun-Han, Bosworth, Ken, 2006. Locally weighted polynomial regression: Parameter choice and application to forecasts of the Great Salt Lake. Water Resour. Res. 42 (5), W05422. http://dx.doi.org/10.1029/2004WR003782.

Lin, Chaoning, Li, Tongchun, Chen, Siyu, Liu, Xiaoqing, Lin, Chuan, Liang, Siling, 2019. Gaussian process regression-based forecasting model of dam deformation. Neural Comput. Appl. 31 (12), 8503–8518. http://dx.doi.org/10.1007/s00521-019-04375-7.

Lu, Zhan-Qian, 1996. Multivariate locally weighted polynomial fitting and partial derivative estimation. J. Multivariate Anal. 59 (2), 187–205. http://dx.doi.org/10.1006/jmva.1996.0060.

Marcelino, Pedro, de Lurdes Antunes, Maria, Fortunato, Eduardo, Gomes, Marta Castilho, 2020. Transfer learning for pavement performance prediction. Int. J. Pav. Res. Technol. 13 (2), 154–167. http://dx.doi.org/10.1007/s42947-019-0096-z.

Marcelino, Pedro, de Lurdes Antunes, Maria, Fortunato, Eduardo, Gomes, Marta Castilho, 2021. Machine learning approach for pavement performance prediction. Int. J. Pav. Eng. 22 (3), 341–354. http://dx.doi.org/10.1080/10298436.2019.1609673.

Marini, Federico, Walczak, Beata, 2015. Particle swarm optimization (PSO), A tutorial. Chemometr. Intell. Lab. Syst. 149 (December), 153–165. http://dx.doi.org/10.1016/j.chemolab.2015.08.020.

Mazari, Mehran, Rodriguez, Daniel D., 2016. Prediction of pavement roughness using a hybrid gene expression programming-neural network technique. J. Traffic Transp. Eng. (Engl. Ed.) 3 (5), 448–455. http://dx.doi.org/10.1016/j.jtte.2016.09.007.

Meshram, Sarita Gajbhiye, Singh, Vijay P., Kisi, Ozgur, Karimi, Vahid, Meshram, Chandrashekhar, 2020. Application of Artificial Neural Networks, support vector machine and multiple model-ANN to sediment yield prediction. Water Resour. Manag. 34 (15), 4561–4575. http://dx.doi.org/10.1007/s11269-020-02672-8.

Momeni, Ehsan, Dowlatshahi, Mohammad Bagher, Omidinasab, Fereydoon, Maizir, Harnedi, Armaghani, Danial Jahed, 2020. Gaussian process regression technique to estimate the pile bearing capacity. Arab. J. Sci. Eng. 45 (10), 8255–8267. http://dx.doi.org/10.1007/s13369-020-04683-4.

Moore, Andrew W., Schneider, Jeff, Deng, Kan, 1997. Efficient locally weighted polynomial regression predictions. In: Proceedings of (ICML) International Conference on Machine Learning. pp. 236–44.

National Cooperative Highway Research Program (NCHRP 1-37A), 2004. Guide for Mechanistic-Empirical Design of New and Rehabilitated Pavement Structures, Appendix Ll-1: Calibration of Fatigue Cracking Models for Flexible Pavements. Transportation Research Board of the National Research Council.

Nguyen, Hoang-Long, Pham, Binh Thai, Son, Le Hoang, Thang, Nguyen Trung, Ly, Hai-Bang, Le, Tien-Thinh, Ho, Lanh Si, Le, Thanh-Hai, Bui, Dieu Tien, 2019. Adaptive network based fuzzy inference system with meta-heuristic optimizations for international roughness index prediction. Appl. Sci. 9 (21), 4715. http://dx.doi.org/10.3390/app9214715.

OBrien, Eugene J., Taheri, Abdolrahim, Malekjafarian, Abdollah, 2018. An alternative roughness index to IRI for flexible pavements. Can. J. Civil Eng. 45 (8), 659–666. http://dx.doi.org/10.1139/cjce-2017-0443.

Patrick, Graeme, Soliman, Haithem, 2019. Roughness prediction models using pavement surface distresses in different Canadian climatic regions. Can. J. Civil Eng. 46 (10), 934–940. http://dx.doi.org/10.1139/cjce-2018-0697.

Pérez-Acebo, Heriberto, Gonzalo-Orden, Hernán, Findley, Daniel J., Rojí, Eduardo, 2021. Modeling the international roughness index performance on semi-rigid pavements in single carriageway roads. Constr. Build. Mater. 272 (February), 121665. http://dx.doi.org/10.1016/j.conbuildmat.2020.121665.

Pérez-Acebo, Heriberto, Linares-Unamunzaga, Alaitz, Rojí, Eduardo, Gonzalo-Orden, Hernán, 2020. IRI performance models for flexible pavements in two-lane roads until first maintenance and/or rehabilitation work. Coatings 10 (2), 97. http://dx.doi.org/10.3390/coatings10020097.

Rajagopalan, Balaji, Lall, Upmanu, 1998. Locally weighted polynomial estimation of spatial precipitation. J. Geogr. Inform. Decis. Anal. 2 (2), 44–51.

Rifai, Andri Irfan, Hadiwardoyo, Sigit P., Correia, Antonio Gomes, Pereira, Paulo, Cortez, Paulo, 2015. The data mining applied for the prediction of highway roughness due to overloaded trucks. Int. J. Technol. 6 (5), 751. http://dx.doi.org/10.14716/ijtech.v6i5.1186.

Shabani, Sevda, Samadianfard, Saeed, Sattari, Mohammad Taghi, Mosavi, Amir, Shamshirband, Shahaboddin, Kmet, Tibor, Várkonyi-Kóczy, Annamária R., 2020. Modeling pan evaporation using Gaussian process regression K-nearest neighbors random forest and support vector machines; Comparative analysis. Atmosphere 11 (1), 66. http://dx.doi.org/10.3390/atmos11010066.

Sholevar, Nima, Golroo, Amir, Sahand Esfahani, Roghani, 2022. Machine learning techniques for pavement condition evaluation. Autom. Constr. 136 (March), 104190. http://dx.doi.org/10.1016/j.autcon.2022.104190.

Terry, Nick, Choe, Youngjun, 2021. Splitting Gaussian processes for computationally-efficient regression. PLoS One 16 (8 August), http://dx.doi.org/10.1371/journal.pone.0256470.

Terzi, Serdal, 2013. Modeling for pavement roughness using the ANFIS approach. Adv. Eng. Softw. 57 (March), 59–64. http://dx.doi.org/10.1016/j.advengsoft.2012.11.013.

The Mathworks Inc., 2016. MATLAB - MathWorks. https://www.Mathworks.Com/Products/Matlab, 2016.

Wang, Zhichen, Guo, Naisheng, Wang, Shuang, Xu, Yang, 2021. Prediction of highway asphalt pavement performance based on Markov chain and Artificial Neural Network approach. J. Supercomput. 77 (2), 1354–1376. http://dx.doi.org/10.1007/s11227-020-03329-4.

Yamany, Mohamed S., Saeed, Tariq Usman, Volovski, Matthew, Ahmed, Anwaar, 2020. Characterizing the performance of interstate flexible pavements using Artificial Neural Networks and random parameters regression. J. Infrastruct. Syst. 26 (2), 04020010. http://dx.doi.org/10.1061/(ASCE)IS.1943-555X.0000542.

Zeiada, Waleed, Dabous, Saleh Abu, Hamad, Khaled, Al-Ruzouq, Rami, Khalil, Mohamad A., 2020. Machine learning for pavement performance modelling in Warm Climate Regions. Arab. J. Sci. Eng. 45 (5), 4091–4109. http://dx.doi.org/10.1007/s13369-020-04398-6.

Zhou, Qingwen, Okte, Egemen, Al-Qadi, Imad L., 2021. Predicting pavement roughness using deep learning algorithms. Transp. Res. Rec.: J. Transp. Res. Board July, http://dx.doi.org/10.1177/03611981211023765, 036119812110237.

Ziari, Hasan, Sobhani, Jafar, Ayoubinejad, Jalal, Hartmann, Timo, 2016. Prediction of IRI in short and long terms for flexible pavements: ANN and GMDH methods Int. J. Pav. Eng. 17 (9), 776–788. http://dx.doi.org/10.1080/10298436.2015.1019498.